Pure Appl. Chem., Vol. 77, No. 12, pp. 2149–2170, 2005.
DOI: 10.1351/pac200577122149
© 2005 IUPAC

INTERNATIONAL UNION OF PURE AND APPLIED CHEMISTRY

PHYSICAL AND BIOPHYSICAL CHEMISTRY DIVISION*

ATOMIC FORCE MICROSCOPY AND DIRECT SURFACE FORCE MEASUREMENTS

(IUPAC Technical Report)

Prepared for publication by
JOHN RALSTON[1,‡], IAN LARSON[2], MARK W. RUTLAND[3], ADAM A. FEILER[4], AND MIEKE KLEIJN[5]

[1]Ian Wark Research Institute, University of South Australia, Mawson Lakes Campus, Adelaide, SA 5095, Australia; [2]Department of Pharmaceutics, Victorian College of Pharmacy, Monash University, 381 Royal Parade, Parkville Vic 3052, Australia; [3]Institute for Surface Chemistry, P.O. Box 5607, 114 86 Stockholm, Sweden; [4]Department of Chemistry, Surface Chemistry, Royal Institute of Technology, 100 44 Stockholm, Sweden; [5]Laboratory of Physical Chemistry and Colloid Science, P.O. Box 8038, 6700 EK Wageningen, The Netherlands

*Membership of the Division Committee during the preparation of this report was as follows:
***President*:** R. D. Weir (Canada, 2004–2005); ***Past-President*:** J. Ralston (Australia, 2002–2003); ***Secretary*:** M. J. Rossi (Switzerland, 2000–2005); ***Titular Members*:** G. H. Atkinson (USA, 2002–2005); W. Baumeister (Germany, 2004–2007); R. Fernandez-Prini (Argentina, 2002–2005); J. G. Frey (UK, 2000–2005); R. M. Lynden-Bell (UK, 2002–2005); J. Maier (Germany, 2002–2005); Z.-Q. Tin (China, 2004–2007); ***Associate Members*:** S. Califano (Italy, 2002–2005); S. Cabral de Menezes (Brazil, 2004–2005); A. J. McQuillan (New Zealand, 2004–2005); D. Platikanov (Bulgaria, 2004–2005); C. A. Royer (France, 2004–2007).

‡Corresponding author: E-mail: John.Ralston@unisa.edu.au

Republication or reproduction of this report or its storage and/or dissemination by electronic means is permitted without the need for formal IUPAC permission on condition that an acknowledgment, with full reference to the source, along with use of the copyright symbol ©, the name IUPAC, and the year of publication, are prominently visible. Publication of a translation into another language is subject to the additional condition of prior approval from the relevant IUPAC National Adhering Organization.

Atomic force microscopy and direct surface force measurements

(IUPAC Technical Report)

Abstract: The atomic force microscope (AFM) is designed to provide high-resolution (in the ideal case, atomic) topographical analysis, applicable to both conducting and nonconducting surfaces. The basic imaging principle is very simple: a sample attached to a piezoelectric positioner is rastered beneath a sharp tip attached to a sensitive cantilever spring. Undulations in the surface lead to deflection of the spring, which is monitored optically. Usually, a feedback loop is employed, which holds the spring deflection constant, and the corresponding movement of the piezoelectric positioner thus generates the image. From this it can be seen that the scanning AFM has all the attributes necessary for the determination of surface and adhesion forces; a sensitive spring to determine the *force*, a piezoelectric crystal to *alter* the separation of the tip and surface, which if sufficiently well-calibrated also allows the *relative separation* of the tip and surface to be calculated. One can routinely quantify both the net surface force (and its separation dependence) as the probe *approaches* the sample, and any adhesion (pull-off) force on *retraction*. Interactions in relevant or practical systems may be studied, and, in such cases, a distinct advantage of the AFM technique is that a particle of interest can be attached to the end of the cantilever and the interaction with a sample of choice can be studied, a method often referred to as colloid probe microscopy. The AFM, or, more correctly, the scanning probe microscope, can thus be used to measure surface and frictional forces, the two foci of this article. There have been a wealth of force and friction measurements performed between an AFM *tip* and a surface, and many of the calibration and analysis issues are identical to those necessary for colloid probe work. We emphasize that this article confines itself primarily to elements of colloid probe measurement using the AFM.

Keywords: AFM; atomic force; colloids; colloid probes; IUPAC Physical and Biophysical Chemistry Division.

INTRODUCTION

The atomic force microscope (AFM) is designed to provide high-resolution (in the ideal case, atomic) topographical analysis, applicable to both conducting and nonconducting surfaces [1,2].

The basic imaging principle is very simple: a sample attached to a piezoelectric positioner is rastered beneath a sharp tip attached to a sensitive cantilever spring. Undulations in the surface lead to deflection of the spring, which is monitored optically. Usually, a feedback loop is employed which holds the spring deflection constant, and the corresponding movement of the piezoelectric positioner thus generates the image. A schematic representation of the technique is shown in Fig. 1. From this, it can be seen that the scanning AFM has all the attributes necessary for the determination of surface and adhesion forces; a sensitive spring to determine the *force*, a piezoelectric crystal to *alter* the separation of the tip and surface, which if sufficiently well-calibrated also allows the *relative separation* of the tip and surface to be calculated. It is customary to disable the in-plane (x,y) motion of the sample and focus solely on sample motion normal to the sample surface (z), although for *frictional* force measurements this is not the case. An example of the raw data obtained for a force measurement is reproduced in

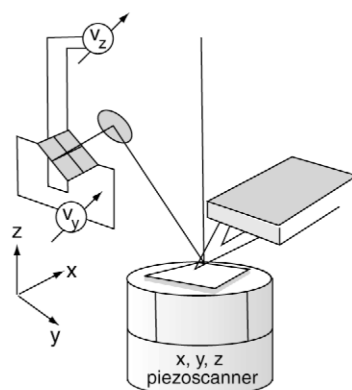

Fig. 1 Schematic diagram of an AFM. The sample is placed on the piezoelectric scanner. A laser is reflected off the upper side of the cantilever and into a split photodiode via a mirror. In this way, vertical (z) and horizontal (y) deflection signals can be measured. For colloid probe microscopy, a well-defined particle is glued to the tip of the cantilever.

Fig. 2. The speed of the piezoscanner can typically be varied over at least a three-orders-of-magnitude range. One can routinely quantify both the net surface force (and its separation dependence) as the probe *approaches* the sample, and any adhesion (pull-off) force on *retraction*. In this respect, there are some obvious parallels to be drawn with the direct force measurement device of Israelachvili and Adams [3]. Measurements with atomically smooth mica with the surface force apparatus (SFA) have resulted in the confirmation of interaction and adhesion theories and have also led to the elucidation of a number of additional forces of varying range, magnitude, and sign that affect the fundamental interaction between surfaces in liquid media [4]. This technique is unparalleled for high-resolution force measurement and has the advantage that the absolute separation of two surfaces can be directly measured. Often, however, it is interactions in relevant or practical systems that are of interest, and in such cases a distinct advantage of the AFM technique is that a particle of interest can be attached to the end of the cantilever and the interaction with a sample of choice can be studied. This important development was pioneered by Ducker et al. [5] and is often referred to as *colloid probe microscopy*. Strictly speaking, a colloidal particle is less than 1 μm in diameter and the particles used in this application are typically in the range 1–20 μm, so this name is technically a misnomer. It is, however, so well established in the literature that we will continue to use this term throughout. The AFM or, more correctly, the scanning probe microscope, can thus be used to measure surface and frictional forces, the two foci of this article. There have been a wealth of force and friction measurements performed between an AFM *tip* and a surface, and many of the calibration and analysis issues are identical to those necessary for colloid probe work. We refer the reader to several admirable reviews [6–9]. We emphasize that this article confines itself primarily to elements of colloid probe measurement using the AFM.

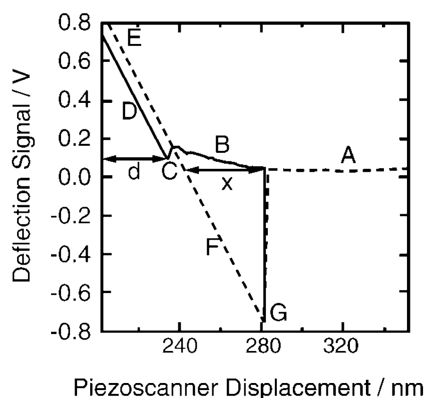

Fig. 2 A typical deflection signal/piezo trace measured in an aqueous electrolyte. When the sphere and the flat are well separated (>100 nm), there is no measurable interaction (A). As the flat approaches the sphere, we observe an initial (B) electrostatic repulsion (upward deflection) followed by a jump into contact (C). Thereafter, the flat and sphere are coupled at (D). At E, the flat is retracted. Hysteresis (F) is observed due to the adhesion between the two surfaces. At G, the removal force exceeds the adhesion and the surfaces separate. In adhesion studies, the key parameters are the pull-off force (F_p) and the loading force, which may be readily calculated. The x (measured along the zero force-deflection line) is the piezoelectric movement required to break sphere-flat contact and d is the piezoscanner movement after contact.

CALIBRATION OF CANTILEVER SPRING CONSTANTS FOR NORMAL (*z*) DEFLECTION

Quantitative force measurements require an accurate value of the cantilever spring constant, which has a Hookean response over the range of deflections encountered in force measurements. In early work, nominal (unmeasured) values supplied by the manufacturers were used [5]. However, these values are seldom better than a rough guide and there is sufficient variation even between cantilevers from the same batch to necessitate their individual calibration. In principle, the spring constant can be calculated from a knowledge of the cantilever's geometrical and material properties [10,11]. A difficulty here is the popularity of V-shaped cantilevers, which are far less easy to model mathematically than the alternative beam-shaped (diving board) cantilevers (see Fig. 3). The most commonly used treatment is the so-called *two-beam approximation*, in which the cantilever is described by two rectangular beams in parallel [12].

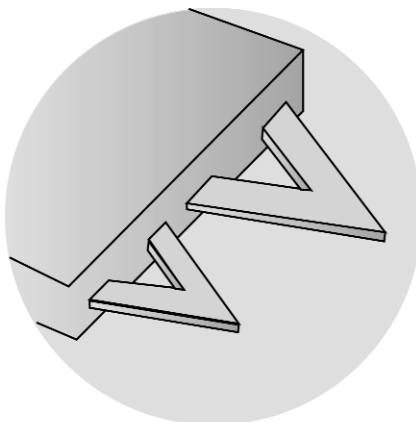

Fig. 3 Schematic depiction of two V-shaped cantilevers. Typically, these are 100 or 200 µm long with a beam width of about 30 µm and of the order of 1 µm thick.

This leads to the following expression for the spring constant k:

$$k = \left(\frac{t}{l}\right)^3 \frac{Ew}{4} \tag{1}$$

in which E is the elastic modulus of the bulk material, and t, w, and l are the thickness, width, and length of the cantilever beams, respectively. The width and length of the cantilever beams can be determined quite accurately from scanning electron microscopy (SEM) images, and the variation in these values for the same type of cantilevers on one wafer is rather small. However, cantilevers are very thin, and there may be variation in the thicknesses of cantilevers from the same batch. Since in eq. 1 the thickness is raised to the power three, small variations in the thickness can lead to large errors in the actual spring constant. Thus, to successfully apply this approach, the thickness would need to be precisely measured. Even if this were simple, the value of the elastic modulus would still not be accurately known. The modulus of a thin cantilever can differ markedly from bulk values due to inhomogeneity, and the presence of a reflective coating of unknown thickness adds further uncertainty.

Sader et al. [11] have performed a finite element analysis of the static deflection of V-shaped cantilevers and presented exact numerical results for the spring constant for a variety of cantilever dimensions. Once again, the thickness and modulus need to be known. Experience proves that such calculated values do not necessarily agree well with accurate experimental ones, thus, direct *measurement* of the k is preferred.

Various methods to measure the cantilever spring constant have been proposed and, for historical reasons, are briefly catalogued here. Butt [7] placed a small pendulum against a vertically mounted cantilever and by slightly tilting the set-up applied an adjustable force to the cantilever. Senden and Ducker [13] proposed a simple method which employs the attachment of a tungsten sphere (10–50 μm in diameter) of known mass to the end of the cantilever. The deflection of the cantilever is measured, and the AFM head is turned upside down, after which the cantilever deflection is measured again. The difference between the two measurements is twice the deflection due to gravity, from which the spring constant can be determined. Many modern commercial AFM heads have automatic shut-offs for safety reasons, which prevent this technique's use.

The spring constant can also be estimated from a power spectral density analysis of the thermal vibration of the free cantilever, i.e., not interacting with a surface [14].

Modeling the cantilever as a harmonic oscillator with one degree of freedom, neglecting higher modes of oscillation [14], it can be shown that

$$k = \frac{k_B T}{\langle z^2 \rangle} \tag{2}$$

in which $\langle z^2 \rangle$ is the mean square deflection of the cantilever due to thermal motion in the vertical direction, k_B the Boltzmann constant, and T the temperature. The value of $\langle z^2 \rangle$ equals the area under the power spectrum of the thermal vibrations in the z-direction. Equation 2 is based on the equipartition theorem, stating that the thermal energy stored in the vibration equals $\frac{1}{2}k_B T$, and the fact that a bending of the cantilever by a small amount of z corresponds to a potential energy of $\frac{1}{2}kz_2$. Butt and Jaschke [15] calculated the thermal noise of a rectangular cantilever with one free end considering all possible vibration modes and showed that the relationship given in eq. 2 is also valid for the total thermal noise. However, in case the fluctuations are measured optically using the reflection of a laser beam on the back of the cantilever, it is not the vertical displacement z, but rather the inclination dz/dx that is measured (x is the coordinate in the longitudinal direction of the cantilever). The relation between inclination dz/dx and displacement z varies for the different modes of vibration since it depends on the shape of the deformations (oscillating shapes differ from the static shape [15]). According to the analysis given by Butt and Jaschke [15], a correction factor of 4/3 has to be included:

$$k = \frac{4k_B T}{3 < z^{*2} >} \tag{3}$$

Here, z^* is the (virtual) displacement as measured using the optical lever technique. A complication is that because of bandwidth limitations only the first modes are experimentally accessible. For a rectangular cantilever, the contribution of the first peak in the noise power spectrum (1st harmonic oscillation) to the virtual deflection is about 70 % [15]. The findings of Butt and Jaschke have been experimentally verified by Lévy and Maaloum [16].

Stark et al. [17] calculated the thermal noise of a V-shaped cantilever by means of a finite element analysis and showed that the thermal noise of V-shaped cantilevers differs systematically from that of rectangular cantilevers. For the cantilever for which the analysis was performed, the contribution of the 1st harmonic oscillation to the noise power spectrum is approximately 78 %. Therefore, using the simplifying assumption of a rectangular beam model in the determination of the spring constant for such a V-shaped cantilever from the first peak in the noise power spectrum would give rise to an error of about 8 %.

The thermal vibration method is an elegant way to evaluate the spring constants of AFM cantilevers and gives fairly accurate results provided that the contributions of the various vibration modes to the noise power spectrum are taken into account. For this, the model of Butt and Jaschke is available in the case of a rectangular cantilever, while for V-shaped cantilevers, a finite element analysis as applied by Stark et al. gives satisfying results. If the AFM software allows for a sufficiently detailed spectral analysis of the thermal noise, the method is also experimentally simple to perform. Determination of the spring constant using this method is not affected by the viscosity of the medium or by the effective mass of the cantilever, which has been experimentally verified by, e.g., Roters and Johannsmann [18]. This allows for calibration directly in the system in which force measurements are performed. By far, the most reliable method for determination of the spring constant involves measurement of the shift in the resonant frequency of the cantilever when loaded with particles of known mass and is often referred to as the Cleveland Method [19].

THE CLEVELAND METHOD

In this method, particles of known size and density are attached to the free end of the cantilever and the spring constant k is determined from the resulting shift of the cantilever's resonant frequency. Using this method, it is not necessary to know the mass of the cantilever itself.

The resonant frequency v_0 of the unloaded cantilever is given by

$$v_0 = \frac{1}{2\pi}\sqrt{\frac{k}{m}} \tag{4}$$

The cantilever is approximated as a spring with a spring constant k and an effective mass m. When a mass M is added to the end of the cantilever, this becomes

$$v = \frac{1}{2\pi}\sqrt{\frac{k}{m+M}} \tag{5}$$

Rearranging this equation gives

$$M = \frac{k}{(2\pi v)^2} - m \tag{6}$$

Thus, measuring the resonant frequencies of the cantilever for various attached masses and plotting M as a function of $(2\pi v)^{-2}$ should give a line with a gradient equal to the spring constant. If desired, the effective cantilever mass follows from the intercept of this plot for $1/v^2 = 0$.

The resonant frequency of the cantilever can be easily determined on a commercial AFM (the imaging technique of tapping mode requires a means of exciting the cantilever and determining its resonant frequency). First, the resonant frequency v_0 of the unloaded cantilever is determined. After this, a particle of known mass is attached to the cantilever, and the resonant frequency is again measured. Attaching the end mass is performed in much the same way as with colloidal probes, only this time, no glue is used (in air, the particles stick due to capillary adhesion). Tungsten spheres with diameters in the range 10–30 μm may be conveniently used as end masses.

In principle, measuring the resonant frequencies of the unloaded cantilever and the loaded cantilever for just one value of M would suffice to calculate k from eqs. 4 and 5. However, in practice, there are small errors in the masses of the spheres (related to determining the precise size of the tungsten particles, thus ±1 to 2 %) and so several loadings are desirable. An example of a linearized spring constant calibration plot is given in Fig. 4.

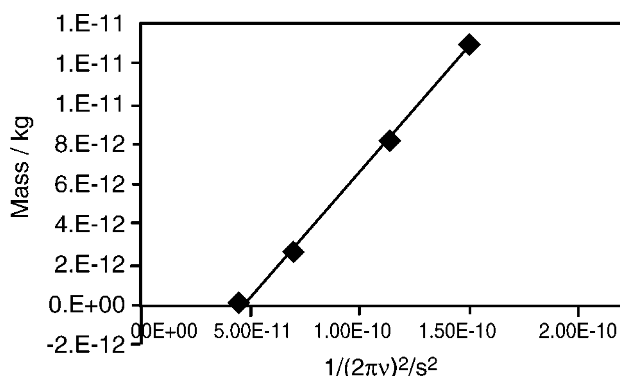

Fig. 4 Typical cantilever calibration plot for a standard 200-μm “wide-legged” cantilever. Spring constant 0.126 N/m.

ESTIMATION OF THE SPRING CONSTANT FROM UNLOADED RESONANT FREQUENCY

For cantilevers differing in thickness but otherwise identical, the spring constants are proportional to the cube of their unloaded resonant frequencies. This is expressed by [19]

$$k = 2\pi^3 l^3 w \rho^{3/2} E^{-1/2} \left(v_0\right)^3 \tag{7}$$

with ρ the (effective) density of the cantilever material, and v_0 the resonant frequency of the unloaded cantilever. The other parameters are defined above.

In Fig. 5, the measured (as in Fig. 4) spring constants of a number of cantilevers originating from the same wafer are plotted against their unloaded resonant frequencies raised to power three. A linear relation is found, indicating that variations in the dimensions (width, length) and elastic properties of these cantilevers are relatively small. Thus, if an accurate spring constant determination is made on a cantilever from a certain batch, the spring constants of other cantilevers in the batch can be *estimated* from their unloaded resonant frequencies. A note of caution should be sounded here—there is no substitute for direct measurement, and the relationship in Fig. 5 is not *always* observed. As an aside, we make the comment that *V-shaped cantilevers* appear to adhere better to such linear relationships than beam cantilevers.

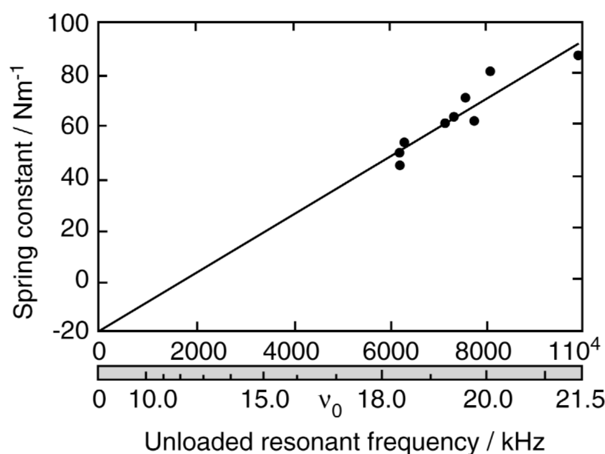

Fig. 5 Spring constants for a number of cantilevers from one wafer plotted against their (resonant frequencies) [3]. The cantilevers used were DI standard contact-mode cantilevers, 200 μm long wide-legged. On the lower horizontal scale, both (resonant frequency) [3] and the corresponding resonant frequency are shown.

CALIBRATION OF THE PIEZOSCANNER

The calibration of the z-piezoscanner movement is also required for the quantitative calculation of both forces and separation. There are two issues with the z-movement of the piezoscanner. Firstly, the degree of expansion for a given applied voltage needs to be known, and, secondly, the nonlinearity and hysteresis of this movement need to be accounted for.

Many commercial AFMs now have closed-loop piezos which automatically take account of the hysteresis, however, this does not solve the issue of how far the piezo expands for a given voltage since this is dependent on the age of the piezo, ambient humidity, *and the rate at which the force curve is performed* [20].

Scanning of calibration samples with well-defined features is one method that can be used to approximate the expansion of the piezo for a given voltage, however, no information on the nonlinearity is obtained. An interferometric method of calibration, proposed by Jaschke and Butt [21], is very convenient and widely used. In this method, the laser beam is positioned so that the beam is split between the end of the cantilever and a reflective substrate (e.g., a polished silicon wafer). The substrate is an-

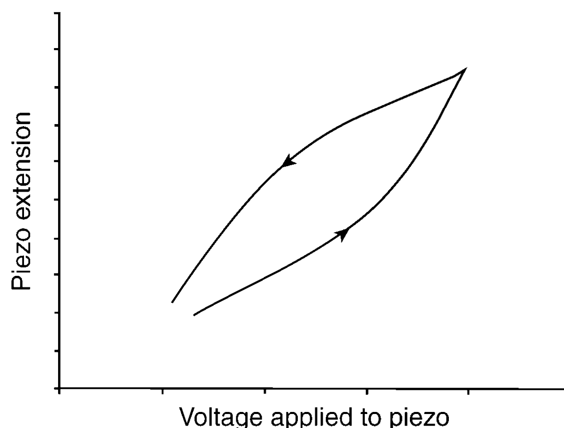

Fig. 6 Schematic showing the piezo reponse to applied voltage. There is a marked hysteresis between the extending and contracting arms of the curve.

gled approximately parallel to the plane of the cantilever with the probe close to the substrate. An interference pattern is generated by light reflecting from the two surfaces as they are moved with respect to one another by cycling the piezo in and out. Since the laser wavelength and path length geometry are known, the true movement of the piezo can be obtained. In some modern commercial devices, however, the use of incoherent lasers renders this approach difficult.

PARTICLE ATTACHMENT

Overview

Particles are typically attached to the end of AFM cantilevers by micromanipulators under an optical microscope. They are glued, with either a chemically inert thermotropic resin, or polymerizable glues (either UV or chemically cured) using a fiber of appropriate size and material properties.

Smooth, spherical colloids are preferable for quantitative measurements (see later discussion). Particles of less well-defined geometry may also be used, but a greater degree of scatter in the measured force data can be expected. In early work, the lower limit to the size of the colloid probes was dictated by the height of the AFM tip (4 µm), but the availability of "tipless" cantilevers removed this particular size restriction and the particle size now depends solely on the resolution of the microscope. In recent work, the attachment methodology has been refined and particles smaller than 1 µm in diameter have been attached and their interactions studied. The majority of colloid probe studies focus on the interaction between a sphere and a flat surface, however, the interaction between two spheres is almost as straightforward [22,23]. Spheres can be attached to a substrate in the same way as to a cantilever, or scattered onto an adhesive surface. With the latter approach, the question of immersion, or partial coating of the substrate particle with glue, needs to be carefully examined. The major challenge of the sphere–sphere case is to ensure that the particles are perfectly aligned, and this can generally be achieved by *scanning* the cantilever particle over the substrate particle, and using the AFM software to position the tip at the center of the resulting spherical image. In this case, a genuinely symmetrical interaction can be achieved.

Attachment procedure

The main elements required to mount particles on cantilevers are shown schematically in Fig. 7. A micromanipulator is used to control the spatial positioning of a fiber with respect to the cantilever, which is placed under a microscope objective lens. (A piezo-actuated micromanipulator can provide submicron precision, but mechanical XYZ stages with, e.g., micron precision are generally more than adequate.) The attachment is a two-step process whereby glue is first transferred to the cantilever (about 10^{-15} l) using a suitable fiber. A second fiber should then be employed to place a particle onto the small patch of glue. Typically, the particles attach spontaneously to the fiber through capillary or van der Waals forces.

Glass filaments [24] and etched tungsten wires [25] have both been commonly employed as the attachment fibers. Etched tungsten wires have long been used as STM tips, and it is the same properties that make them attractive for particle attachment—a suitably fine point for accurate glue placement and high rigidity. A recipe for their manufacture is briefly elaborated here. A tungsten wire (e.g., 0.25 mm diameter) can be etched by immersing one end in 1 M KOH and applying a d.c. voltage of a few tens of volts between the wire attached to the positive terminal and a platinum electrode (cathode) placed elsewhere in the solution. This rapidly reduces the end diameter to the order of 1 µm thickness. After etching, the wire is rinsed in water and ethanol, dried in a stream of nitrogen, and clamped in the micromanipulator.

The most popular glue choice is a heat-softening epoxy resin such as Epikote 1004 with melting point roughly 100 °C. This has been shown not to cause contamination through dissolution in water.

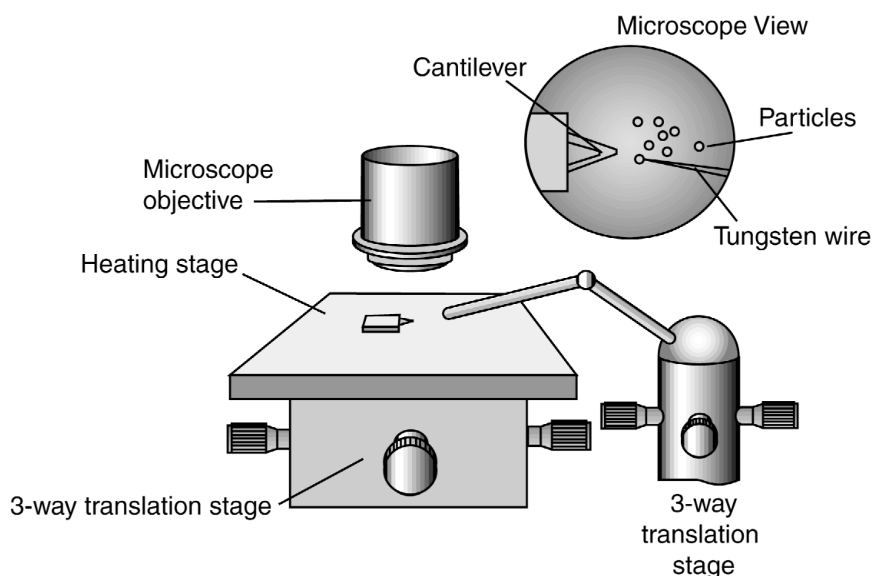

Fig. 7 Apparatus used to glue particles to the end of AFM cantilevers.

However, its use requires a heating stage, which is an additional complication, and, more importantly, overheating of the cantilever may cause permanent damage. This approach is only suitable for particles that will not be affected by the relatively high temperature.

Some representative pictures of the results are shown in Fig. 8.

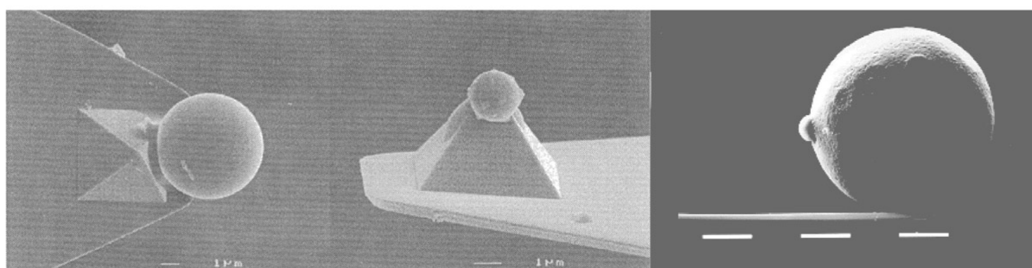

Fig. 8 SEMs of particles glued to AFM cantilevers. The left-hand image shows a 6-µm silica particle attached in the standard way, whereas the middle image shows a 1.5-µm silica particle attached to the top of the cantilever tip. The right-hand image shows a 20-µm cellulose bead attached to a tipless cantilever.

FORCE MEASUREMENTS

A force measurement is made by ramping the probe and substrate together and monitoring cantilever deflection as a function of displacement. In some devices, the cantilever is mounted on the piezo and it is the probe that is moved, in other devices, it is the substrate that is ramped. An example of the latter case is depicted in Fig. 9.

The types of forces that may act between the surfaces and their characteristic distance dependences are fully documented elsewhere [4,8,26]. These forces acting between the surfaces cause the cantilever to deflect prior to their physical contact. The vertical axis of Fig. 9 shows the output of the photodiode, whilst the horizontal axis shows the position of the piezo. The curve I-II-III shows the interaction on approach and the other (in this case with a deep adhesive minimum) corresponds to the inter-

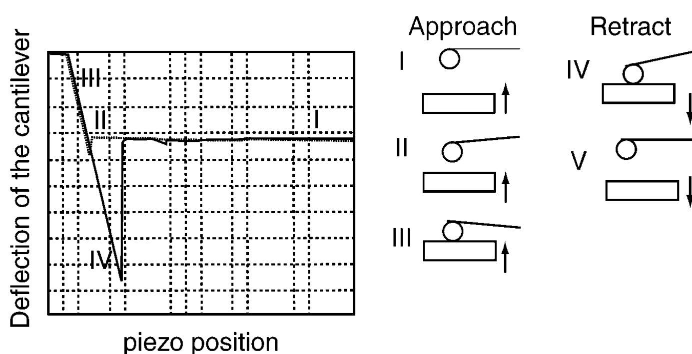

Fig. 9 A typical force graph in which the deflection of the cantilever is plotted against the piezo position. On the right, the position of the colloidal probe and the flat surface on the piezo are shown for several points of the curve, indicated by Roman numerals.

action upon retraction. At large distance (I), no force acts on the particle. At shorter separations (II), a surface force may be experienced either as an attraction (as in Fig. 9) or repulsion. When the particle and flat surface come into physical contact, the probe movement complies with the movement of the piezo. It is this linear region that is used to calibrate the deflection voltage in terms of distance units (III). This part of the curve is often called the *constant compliance region*. The piezo movement is then reversed. If the contact is adhesive (almost always the case in air, for example), then the surfaces remain in contact until the restoring force in the spring overwhelms the adhesive force (IV) and the surfaces snap apart.

We note that for hydrodynamic studies and interactions of polymer-bearing surfaces, a rather high resolution and novel *dynamic* method has been developed by Notley et al. [27]. The analysis of such measurements is rather different than for the static method elaborated in this article, and we will not pursue this any further except to say that the technique is based on an oscillating substrate, and instead of obtaining the force from the static deflection of the cantilever, the phase difference of the cantilever's oscillation is used.

CONSTRUCTION OF FORCE VS. DISTANCE CURVES

The photodiode *voltage vs. piezo position* curve can be converted into a *force vs. distance* curve, in which the force (in Newtons) is plotted against the actual distance between the surfaces (see Fig. 10).

There are several steps involved in the conversion process.

1. The arbitrary photodiode voltage at large separations (I,V) actually corresponds to "zero deflection", so this value (usually obtained by averaging over an appropriately large region) should just be subtracted from the entire curve.
2. The gradient of the constant compliance region can then be used to convert the photodiode signal to deflections in nanometres. This region also in practice defines the point of zero separation.
3. The separation of the surfaces is then obtained from the combined movements of the piezo and cantilever.
4. Finally, the cantilever deflection is converted to force using Hookes' law and the measured spring constant (described earlier).

It should be noted, however, that constant compliance only provides a relative zero of separation, since it is impossible to know whether true contact, as opposed to contact of rigidly adsorbed layers, is achieved. Furthermore, if one or both of the surfaces are compressible, then physical contact occurs before constant compliance occurs. Particular care should be taken here because often an apparently lin-

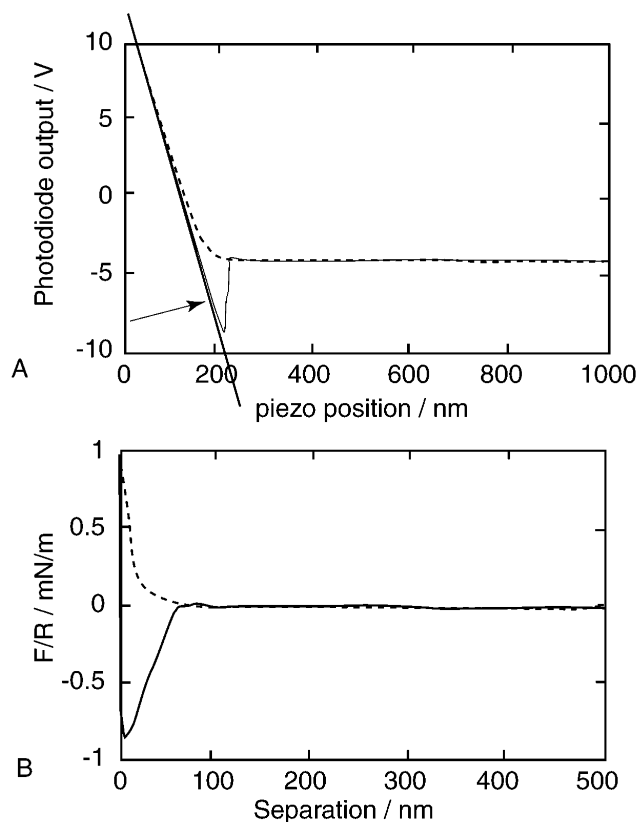

Fig. 10 The raw data graph (A) is converted to a force distance graph (B). The dashed curve is the interaction on approach, and the continuous curve is the interaction on retraction. In graph A, the constant compliance region for the retraction is marked.

ear regime can occur in such systems, which can lead to errors in both force and separation. The gradient of the constant compliance region should thus be taken at as high loads as possible. Other aspects of deformable surfaces are discussed later.

Caution should be taken at high applied loads since the photodiode signal becomes highly nonlinear with deflection. In general, a photodiode will only be linear with deflection over a limited central range. While the nonlinearity of the photodiode can be calibrated, such an approach is only valid for a single laser spot alignment. An external measure of the piezo movement is also required for such a calibration. Thus, stiffer springs are often preferred, though this compromises resolution and may lead to damage of softer biological samples.

Force distance curves recorded as above are dependent on the specific geometry of the probe and surface employed. To allow comparison between different measurements, and fitting of interaction theories, it is convenient to normalize the measured force by the measured radius for reasons outlined in the next section.

GEOMETRY OF THE INTERACTION

Usually, the interaction is displayed as a force divided by an effective interaction radius R, in units of Newtons per metre. This quantity is related to the interaction free energy per unit area $G_f(D)$, between equivalent flat surfaces at separation D, by

$$F(D)/R = 2\pi G_f(D) \tag{8}$$

This relation is known as the *Derjaguin approximation* [28]. It is valid provided that $R >> D$, the surface separation, and provided that R is independent of D. The effective radius is defined as:

$$R = \left(\frac{R_1 R_2}{R_1 + R_2}\right) \tag{9}$$

where R_1 and R_2 are the spherical radii of the two surfaces. For a smooth sphere–surface interaction, R is just the sphere radius ($R_2 = \infty$), whereas for the interaction between two identical spheres, the effective radius is half that of the individual spheres. Normalization of the interaction force in this way facilitates comparison of force measurements performed with colloidal probes of different sizes or in systems with different geometries. Furthermore, most theoretical descriptions of surface interactions can be readily calculated as a free energy between flat surfaces and is thus convenient for direct comparison of measurements with theory. Strictly speaking, it would be less confusing to plot $F/2\pi R$ rather than F/R, and this is indeed often done, but historically it is more usual to plot F/R.

The radius is most commonly obtained from an SEM image after the experiment is complete since this requires the deposition of a conducting layer. One problem encountered in using electron microscopy to obtain the radius is that the measurement is performed in vacuum. The actual radius under the conditions of the force measurements, for example, when performed in a liquid, may be quite different due, for example, to swelling [29]. With the use of environmental SEM it is possible to obtain images without evaporating a conducting coating. For large particles and high-resolution optical microscopes, it is possible to obtain the radius directly. Another useful method for in situ measurement of the radius is *reverse imaging*, whereby the probe is used to image a sharp feature on the substrate, which results in an image of the particle itself. (This is useful provided that the particle is not so soft that it is damaged by the sharp feature!) It is also the only option for very small probes, such as AFM tips where the radius cannot be obtained from SEM. An advantage of this latter approach is that the true local radius of curvature is obtained (assuming that the sharp feature is truly sharp), which may not necessarily reflect the global curvature of the particle. [Note that when imaging features of a similar curvature to the tip itself, the recorded image is a composite of both the feature and the tip, necessitating a reconstruction if a true image of the feature is to be obtained.]

A misinterpretation of the radius of interaction will affect only the magnitude of F/R (the *shape* of the force profile will not be affected), but this will affect the value of derived parameters such as, for example, the surface potential and charge, Hamaker constant, and the adhesion. For measurements between iron oxide and silica, Toikka et al. concluded that the results could only be interpreted in terms of the local curvature and that the macroscopic particle radius was irrelevant [25].

Seldom is a roughness factor quoted for particles themselves—even if an unambiguous zero of separation can be determined from a force curve, the question still needs to be posed as to exactly what is "contact" for two rough surfaces. For example, the plane of charge, which for mica surfaces can be conveniently defined at the atomically smooth oxide surface, cannot be as well defined for a rough particle, which may locally have nanometre roughness. The attenuation of surface force measurement by surface roughness has been treated for adhesion [30,31], DLVO forces [25], and capillary condensation [32].

Finally, the effects of deformation of the surfaces which arise during measurement need to be considered. When the surfaces are being deformed due to the action of surface forces, the measurement of surface forces becomes highly complicated. As the surfaces deform, both the local radius (which affects the magnitude of the calculated surface force/energy via the Derjaguin approximation) and the relative separation of surfaces change in a way that cannot always be readily determined. Furthermore, deformations may depend on the rate at which the experiments are performed [33]. To be able to interpret force curves, the effects of deformation need to be *calculated* since there is no means of directly ob-

taining this information during the measurement itself. This field is unfortunately vast in itself, and so only a few signposts are offered here. Fortunately, Cappella and Dietler have devoted much effort to these issues in their exhaustive review [6].

There are several contact deformational approaches to estimate the central displacement, δ, due to deformation of two bodies in contact. The simplest description is Hertz theory, which describes deformation of noninteracting elastic spheres of the same material [34]. Assuming no adhesion between the surfaces, it gives the central displacement (or degree of compression) as

$$\delta = \frac{a^2}{R} = \left[\frac{3}{2} \frac{\left(1-\nu^2\right)}{E} \frac{F}{\sqrt{R}} \right]^{\frac{2}{3}} \tag{10}$$

where a is the radius of the flattened contact area, E is Young's modulus, ν is the Poisson ratio, and F is the applied force. JKR (Johnson, Kendall, Roberts) theory [32] extends this theory to account for adhesion in the contact zone

$$a^3 = \frac{3\left(1-\nu^2\right)R}{2E} \left\{ F + 3\pi\gamma R + \left[6\pi\gamma RF + \left(3\pi\gamma R\right)^2 \right]^{1/2} \right\} \tag{11}$$

where γ is the surface energy of the contact area and the central displacement as

$$\delta = \frac{a^2}{R} - \left[4\pi\gamma a \frac{\left(1-\nu^2\right)}{E} \right]^{1/2} \tag{12}$$

The assumption made in the JKR theory that the interactions between the surfaces are infinitely short-ranged has the physically unacceptable result that at the border of the contact region the tensile stress is infinite. An alternative treatment has been proposed which assumes a Hertzian profile and takes into account interactions outside the contact zone (DMT theory) [35]. The DMT theory is expected to be most accurate for small radii, low surface energies, and hard surfaces, whereas the JKR theory is approached when the radii, surface energies, and the softness of the surfaces increase. In fact, these two theories are limiting cases of more recent continuum theories [36–38].

The JKR and DMT theories also differ in the predicted pull-off force; two spheres in adhesive contact will separate exactly at the applied (negative) forces

$$F_s = -\frac{3}{2}\gamma\pi R \qquad \text{(JKR)} \tag{13}$$

$$F_s = -2\gamma\pi R \qquad \text{(DMT)} \tag{14}$$

The central displacement, δ, under the action of strong attractive forces depends, of course, on the radius of curvature, and this is unlikely ever to be more than a few angstroms, for colloid probe measurements employing elastic substrates such as silica. For softer surfaces, this deformation can extend well into the nanometre range.

For systems involving viscoelastic, liquid, or gaseous systems, other considerations are required. AFM measurements involving a solid particle and a bubble [39–42] or droplet [43–45] have been performed. The theoretical challenge presented by these measurements is to describe, in the calculation of force(s), for deformation of the interface and to define the correct interfacial separation. In one approach, the linear Poisson–Boltzmann equation for rigid bodies at large separation has been used to establish the zero of experimental separation, requiring an independent determination of the surface po-

tential [45]. An alternative method involves solving the Young–Laplace equation to deduce the shape of the force–distance curves [46]. In a third approach, the small change in the mean radius of curvature of a drop (or bubble), which in turn is proportional to the small change in fluid pressure involving the drop (or bubble), has been calculated in order to obtain the force between a particle and the drop (or bubble) in question [47]. Perturbation theory has been used, with rather different outcomes [47–49], supplemented by nonperturbative, semi-analytical, and numerical solutions to the Young–Laplace equation. Resolving the differences between these various theoretical descriptions of force–distance profiles, in our view, awaits the accurate experimental determination of interfacial separation. In this regard, interferometry, evanescent wave, and capacitance techniques hold considerable promise.

FRICTIONAL FORCES

Despite the early recognition of the potential of the AFM for friction force measurement [50,51] it was some time before this application became routine for quantifying shear or frictional forces between a tip [51–55], or a particle [56–59], and a sample. As with normal forces, friction can be measured in liquid [56,58,60], air/vapor [57,61,62], or vacuum [42]. In the case where a tip has been modified with a specific functionality, the so-called lateral force microscopy technique is often referred to as chemical force microscopy [52,63,64]. In lateral force mode and colloid probe frictional studies, the fast scan direction is orthogonal to the long axis of the cantilever* and the lateral deflection of the cantilever is monitored by the horizontal photodiodes. A typical trace of lateral deflection signal vs. *y*-piezomovement for a colloid probe is reproduced in Fig. 11. The initial linear region corresponds to static friction, where the surfaces do not move relative to one another, despite the lateral movement applied through the piezo. At some value of the lateral deflection, the surfaces start to slide and the value of the kinetic frictional force is obtained from the difference between the lateral deflection while sliding, and the undeflected value. In practice, it is simplest to find the average value of the deflection while sliding in each direction, take the difference between these values, and divide it by two. This obviates the need to know the undeflected value and (if the static friction portion of the data is rejected) allows simple data analysis routines to be written which can be batch-processed. We note that in the majority of friction measurement techniques, a static friction force *higher* than the sliding friction is observed. That is to say that a sharp maximum is often observed prior to the onset of sliding, which can be considerably larger in magnitude. Stick-slip friction may also be observed in such cases, depending on the mechanical response of the system. In colloidal probe studies, however, the stick maximum is seldom seen and a smooth progression into the kinetic regime is generally observed. It is, thus, rather easy to make the mistake of bundling these two parameters into a single value. The noise in the sliding regime is typical and may be related to stick-slip behavior, although this is generally regular in period when it occurs. It is useful to monitor the normal deflection signal of the cantilever simultaneously, since this will give a clue as to whether the noise reflects topographical features or not. Another trick is to take a lateral force image with the slow scan direction disabled, thus, each new line on the image should be the same track. If features appear parallel to the "slow scan axis", then this indicates reproducibility from scan to scan; if the "image" is featureless, then the noise is most probably random.

Quantitative measurements of friction clearly rely on an accurate conversion of photodiode signal to force units, which requires the lateral, or torsional, spring constant, k_1, to be known. The methodology for determination of k_1 is not as straightforward as for the normal spring constant, k_n, and, consequently, there is as yet no "standard" procedure.

*For standard imaging, the fast scan direction is parallel to the cantilever apex so as to minimize cantilever twist.

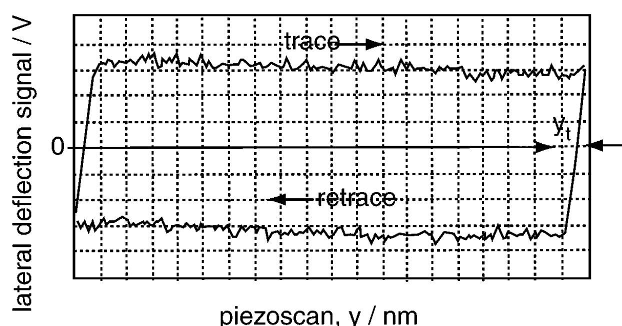

Fig. 11 A typical lateral deflection signal trace measured as a function of the cyclic *y*-piezoscanner travel (500 nm travel in this case). Initially, there is no relative movement between the colloid probe and sample until the lateral force exceeds the static friction. The magnitude of this force can be readily calculated if the probe geometry and lateral spring constant, k_1, are known.

Many proponents of the friction technique *calculate* the torsional spring constant rather than measure it directly. Neumeister and Ducker [10] have proposed a method for the calculation of k_1 by combining an experimentally determined k_n with the more readily measured geometrical parameters for a typical triangular cantilever.

Unfortunately, such calculations are plagued by the same uncertainties in coating properties and thickness value as discussed earlier for normal spring constants. While this is not a catastrophic problem for comparative studies (measurements made with same cantilever) the absolute values are not reliable. Although laborious, it is thus preferable to measure the spring constant directly. Bogdanovic et al. [65] have developed a relatively simple technique involving pressing the cantilever against the sharp tip of a second cantilever mounted upside down on a substrate (there are also many commercial calibration grids, which have sharp features suitable for this) and measuring the deflection–load relationship for various distances from the central axis. This technique is really only suitable for beam cantilevers and Feiler et al. [66] have developed an alternative technique to allow measurement of triangular cantilevers also. A glass fiber of known length is glued to the cantilever, and the twist of the cantilever is measured as a function of normal deflection. The extra lever arm gives improved resolution, but capillary condensation can cause difficulties. Also, the lever must be removed prior to use. Direct comparisons of the two techniques on the same (beam) cantilever have shown that the same value for the spring constant is obtained. Perhaps the most promising experimental approach is that of Sader et al. [11], where the spring constant can be unambiguously obtained from a measurement of the resonant frequencies of torsional and flexural vibrations of the cantilever in air. Numerous other approaches have been suggested, with varying degrees of success and applicability to the colloid probe technique, and have been compared and discussed in recent reviews [66,67].

In general, the maximum applied loads during friction measurement are considerably larger than those of interest for normal force measurement. Thus, the issue of the nonlinearity of the photodiode signal with deflection, discussed earlier for force measurements, becomes even more significant. For this reason, the choice of cantilever stiffness is important. A compromise needs to be made between the ability to apply large loads while remaining in the linear regime, and having sufficient resolution to measure normal forces during the same experiment.

The colloid probe technique has proved useful for studies of interfacial friction at a fairly fundamental level. For example, the effects of adsorbed polymer conformation [68–70], adsorbed salivary protein [71], surfactant aggregate structure [72], roughness [73], and surface chemistry [57,74] have all been studied.

In general, linear friction–load relationships such as that seen in Fig. 12 are observed, and the friction coefficient (the gradient of the line) describes the extent of the friction. For example, the friction

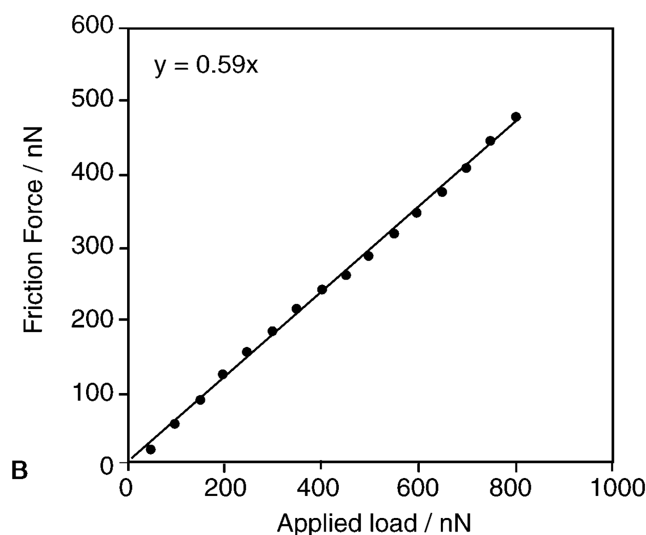

Fig. 12 A typical friction–load relationship between two surfaces in liquid where no attractive force is manifested. The linear relationship is consistent with Amontons' law.

coefficient for two silica surfaces sliding in aqueous solution is about 0.6 [58,71], whereas when lubricating salivary proteins adsorb, the friction is reduced to about 0.03 [71]. Such observations, while characterizing the friction, say nothing about the mechanisms per se. The fact that Amontons' law relates the friction force only to the applied load, independently of the contact area, has caused a certain amount of perplexity over the years. In fact, as has now been shown [75], not least by colloidal probe measurements of friction [57], that the measured frictional force *is* related to the contact area. Sometimes, a relationship such as that seen in Fig. 13 is observed. The behavior can be explained in terms of an adhesive single asperity contact (only one point of contact) where the contact area can be calculated from contact mechanical theories (e.g., JKR discussed earlier). The frictional force at low loads can be shown to be linearly proportional to the calculated contact area, and not the applied load. Amontonsian behavior is thus rationalized by the fact that in general there are a multiplicity of contact points and as the load is increased, so does the number of contacts. It turns out that for large numbers of contacts, the true area of contact varies linearly with the load! For repulsive single asperity systems, the Amontonsian behavior is explained in terms of the high load limit [76] of the Cobblestone [77] model of friction. We note that at the time of writing there is as yet no unified picture of the actual dissipative mechanism of interfacial (non-wear) friction.

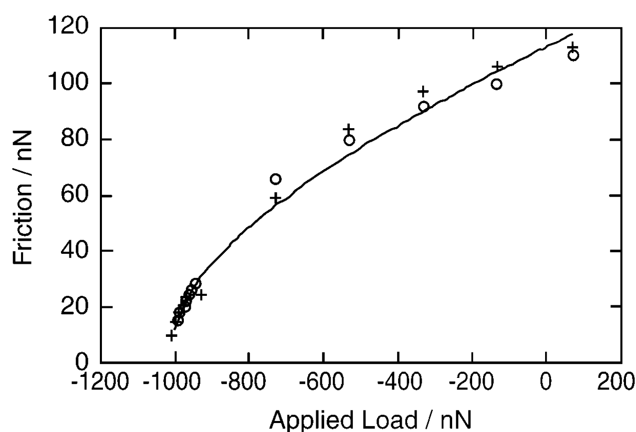

Fig. 13 Nonlinear relationship between friction and load observed for a single asperity contact between cellulose and silica. The negative applied load is due to the fact that the interaction is strongly adhesive—the surfaces separate below about –1 µN. The line is a fit of contact mechanical theory to the data and assumes that there is a linear relationship between friction and the calculated area.

DIFFERENT MATERIALS

Numerous materials other than silicon nitride and silica have been used in AFM force measurements. Butt conducted experiments between diamond surfaces in his original colloid probe paper [7], published the same year as Ducker et al. [5]. Karaman et al. [78] studied the emulsion polymerization of polystyrene and Larson et al. [79] compared results from AFM force measurements between titania surfaces with electrokinetic experiments. Interactions between gold surfaces with and without specific additives [5,24,80–82], zirconia surfaces in the presence of aqueous electrolyte, trisodium citrate, and polyacrylic acid [83–85], α-alumina, and gibbsite surfaces in aqueous electrolyte solutions [86] and between titania and silica surfaces in aqueous linear polyphosphate solutions [87] have also been conducted. Rutland has used cellulose to investigate paper-relevant interactions in both the normal and shear directions [22,29,57].

Biological and polymeric surfaces are increasingly of interest. For example, Bowen et al. [88–90] have studied spore adhesion by gluing a spore to an AFM cantilever and have similarly studied biological adhesion to membrane surfaces. Pashley and colleagues [91] have also studied the interactions between toxic spores in water with a view to their effective flocculation.

When comparing AFM force experiments between identical surfaces in dilute 1-1 electrolyte aqueous solution to electrical double-layer theory, there is only one free parameter: the diffuse layer potential of the surface being studied. The other input is the known electrolyte concentration. If measurements are made between different materials, the diffuse layer potential of each surface is unknown. In Fig. 14, we show theoretical force–separation curves for different pairs of potentials that, when multiplied together, give the same number. At large separations, where theory is fitted to the experimental data, there is little difference between the theoretical curves produced by the various pairs of potentials; there is not a unique pair of potentials that fit the individual force curves. It is, therefore, necessary to obtain independently (preferably by a different technique) the potential of at least one of the surfaces for comparison. Systems such as zinc sulfide-mica [92], silica-titania [93], silica-polypropylene [94], silica-mica [23,95], and silica-alumina [96,97] have all been studied. In refs. [23,97], both surfaces used in the AFM measurements were characterized separately by traditional electrokinetic techniques, allowing a full comparison with the AFM results. These two papers convincingly showed agreement between the potentials derived from the AFM experiments and those obtained from electrokinetic techniques. Hu and Bard performed experiments between a silica colloid probe and a carboxylic acid

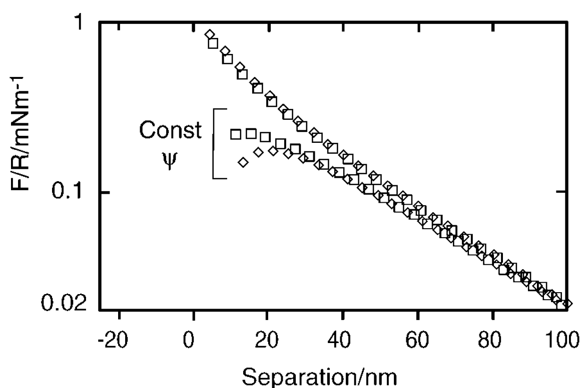

Fig. 14 Theoretical force-separation curves for different pairs of potentials that when multiplied together give the same number. The upper three curves are the constant charge limits, while the lower three are the constant potential boundary conditions. There is very little difference between the constant charge curves, and at large separations there is very little difference between the three constant potential curves.

terminated self–assembled monolayer on a gold substrate [98]. They then extended this work to study the adsorption of SDS on gold surfaces covered with self-assembled monolayers [98]. In both cases, the potential of the silica probe was determined by silica/silica AFM force measurements. While the double layer force is only one of many forces manifested in colloid probe measurement, it underlines the importance of performing experiments in both the symmetrical and asymmetrical cases, if the forces are to be interpreted in terms of the surface properties.

AFM force measurements are certainly not limited to hard, nondeformable surfaces. Butt [39] has performed measurements between silica particles and air bubbles, as have Ducker et al. [40] and Fielden et al. [41]. Interactions between silica colloid probes and oil drops have also been measured [99,100], with droplet–droplet and bubble–bubble interactions next in line. There is great potential, through the use of, say, functionalized carbon nanotube probes, to measure short-range, localized interactions of key importance in biological systems [101].

In all of the studies mentioned so far, the properties of the surfaces, i.e., the diffuse layer potential and diffuse layer charge, have remained constant with time. The AFM force measurement technique has also been shown to be able to measure systems in which both the charge and potential vary as a function of time [102]. In addition, it is also possible to conduct measurements between a colloid probe and a metal or semiconductor surface, whose electrochemical properties are controlled by the experimentalist [103–105]. For example, Raiteri et al. [103] studied the interactions between a silicon nitride tip and gold and platinum surfaces, whilst Hillier et al. [104] used a silica colloid probe and a gold surface. Larson and Pugh have also conducted measurements in the presence of hydrolyzable metal ions in which the adsorption of these ions is seen to change the double-layer repulsion to attraction [106].

ACKNOWLEDGMENTS

The assistance of M. Fielden, G. Toikka, M. Giesbers, and B. Smith in the preparation of the figures and diagrams is gratefully acknowledged.

REFERENCES

1. G. Binnig, C. Quate, G. Gerber. *Phys. Rev. Lett*. **56**, 930 (1986).
2. G. Binnig and H. Rohrer. *Helv. Phys. Acta* **55**, 726 (1982).
3. J. N. Israelachvili and G. E. Adams. *Nature* **262**, 774 (1976).
4. J. N. Israelachvili. *Intermolecular and Surface Forces*, Academic Press, London (1991).
5. W. A. Ducker, T. J. Senden, R. M. Pashley. *Nature* **353**, 239 (1991).
6. B. Cappella and G. Dietler. *Surf. Sci. Rep*. **34**, 1 (1999).
7. H.-J. Butt. *Biophys. J.* **60**, 1438 (1991).
8. P. G. Hartley. In *Colloid-Polymer Interactions*, R. S. Farinato and P. L. Dubin (Eds.), p. 253, John Wiley, New York (1999).
9. R. A. Hayes and J. Ralston. In *Adhesion Promotion Techniques*, K. L. Mittal and A. Pizzi (Eds.), Marcel Dekker, New York (1999).
10. J. M. Neumeister and W. A. Ducker. *Rev. Sci. Instrum*. **65**, 2527 (1994).
11. J. E. Sader, I. Larson, P. Mulvaney, L. R. White. *Rev. Sci. Instrum*. **66**, 3789 (1995).
12. J. E. Sader. *Rev. Sci. Instrum*. **66**, 4583 (1995).
13. T. J. Senden and W. A. Ducker. *Langmuir* **10**, 1003 (1994).
14. J. L. Hutter and J. Bechhoefer. *Rev. Sci. Instrum*. **64**, 1868 (1993).
15. H.-J. Butt and M. Jaschke. *Nanotechnology* **6**, 1 (1995).
16. R. Levy and M. Maaloum. *Nanotechnology* **13**, 33 (2002).
17. R. W. Stark, T. Drobek, W. M. Heckl. *Ultramicroscopy* **86**, 207 (2001).
18. A. Roters and D. J. Johannsmann. *Phys. Condens. Matter* **8**, 7561 (1996).
19. J. P. Cleveland, S. Manne, D. Bocek, P. K. Hansma. *Rev. Sci. Instrum*. **64**, 403 (1993).
20. M. W. Rutland, J. Tyrell, P. Attard. *J. Adhes. Sci. Technol*. **18** (10), 1199–1215 (2004).
21. M. Jaschke and H. Butt. *Rev. Sci. Instrum*. **66**, 1258 (1995).
22. M. W. Rutland, A. Carambassis, G. A. Willing, R. D. Neuman. *Colloids Surf., A* **123–124**, 369 (1997).
23. P. G. Hartley, I. Larson, P. J. Scales. *Langmuir* **13**, 2207 (1997).
24. W. A. Ducker, T. J. Senden, R. M. Pashley. *Langmuir* **8**, 1831 (1992).
25. G. Toikka, R. Hayes, J. J. Ralston. *Colloid Interface Sci.* **180**, 339 (1996).
26. P. M. Claesson and M. W. Rutland. In *Handbook of Applied Colloid and Surface Chemistry*, K. Holmberg (Ed.), John Wiley, Chichester (2002).
27. S. M. Notley, S. Biggs, V. S. Craig. *J. Macromolecules* **36**, 2903 (2003).
28. B. V. Derjaguin. *Kolloid-Z.* **69**, 155 1934.
29. A. Carambassis and M. W. Rutland. *Langmuir* **19**, 5584 (1999).
30. Y. J. Rabinovich. *Colloid Interface Sci.* **232**, 1 (2000).
31. Y. Rabinovich, J. Adler, M. Esayanur, A. Ata, R. Singh, B. Moudgil. *Adv. Colloid Interface Sci.* **96**, 213 (2002).
32. K. L. Johnson, K. Kendall, A. D. Roberts. *Proc. R. Soc. London, Ser. A* **324**, 301 (1971).
33. P. Attard, J. C. Schulz, M. W. Rutland. *Rev. Sci. Instrum*. **69**, 3852 (1998).
34. H. J. Hertz. *Reine Angew. Math*. **92**, 156 (1881).
35. B. V. Derjaguin, V. M. Muller, Y. P. Toporov. *J. Colloid Interface Sci*. **53**, 314 (1975).
36. M. Barquins and D. Maugis. *J. Méc. Theor. Appl.* **1**, 331 (1982).
37. D. Maugis. *J. Colloid Interface Sci*. **150**, 243 (1992).
38. N. Burnham and R. J. Colton. *J. Vac. Sci. Technol.* **7**, 2906 (1989).
39. H. J. Butt. *J. Colloid Interface Sci.* **166**, 109 (1994).
40. W. A. Ducker, Z. G. Xu, J. N. Israelachvili. *Langmuir* **10**, 3279 (1994).
41. M. L. Fielden, R. A. Hayes, J. Ralston. *Langmuir* **12**, 3721 (1996).
42. M. Preuss and H. J. Butt. *Langmuir* **14**, 3164 (1998).
43. P. G. Hartley, F. Grieser, P. Mulvaney, G. W. Stevens. *Langmuir* **15**, 7282 (1999).

44. S. A. Nespolo, D. Y. C. Chan, F. Grieser, P. Hartley, G. W. Stevens. *Langmuir* **19**, 2124 (2003).
45. G. Gillies, C. A. Prestidge, P. Attard. *Langmuir* **18**, 1674 (2002).
46. D. Bhatt, J. Newman, C. J. Radke. *Langmuir* **17**, 116 (2001).
47. D. C. Bardos. *Surf. Sci*. **517**, 157 (2002).
48. P. Attard and S. Miklavcic. *J. Colloid Interface Sci*. **247**, 255 (2002).
49. P. Attard and S. Miklavcic. *Langmuir* **17**, 8217 (2001).
50. G. Meyer and N. M. Amer. *Appl. Phys. Lett*. **57**, 2089 (1990).
51. Y. H. Liu, T. Wu, D. Evans. *Langmuir* 10 (1994).
52. R. W. Carpick, N. Agrait, D. F. Ogletree, M. Salmeron. *J. Vac. Sci. Technol. B* **14**, 1289 (1996).
53. R. W. Carpick, N. Agrait, D. F. Ogletree, M. Salmeron. *Langmuir* **12**, 3334 (1996).
54. R. Carpick, D. Ogletree, M. Salmeron. *J. Colloid Interface Sci.* **211**, 395 (1998).
55. B. Bhushan and C. Dandavate. *J. Appl Phys.* **87**, 1201 (1999).
56. G. Toikka, R. A. Hayes, J. Ralston. *J. Adhes. Sci. Technol.* **11**, 1479 (1997).
57. G. Bogdanovic, F. Tiberg, M. W. Rutland. *Langmuir* **17**, 5911 (2001).
58. A. Feiler, I. Larson, P. Jenkins, P. Attard. *Langmuir* **16**, 10269 (2000).
59. A. Meurk, J. Yanez, L. Bergstrom. *Powder Technol*. **119**, 241 (2001).
60. M. A. Plunkett, P. M. Claesson, M. Ernstsson, M. W. Rutland. *Langmuir* **19**, 4673 (2003).
61. S. Ecke and H. Butt. *J. Colloid Interface Sci*. **244**, 432 (2001).
62. S. Biggs, R. Cain, N. Page. *J. Colloid Interface Sci*. **232**, 133 (2000).
63. C. D. Frisbie, L. F. Rozsnyai, A. Noy, M. S. Wrighton, C. M. Lieber. *Science* **265**, 5181, 2071 (1994).
64. S. C. Clear and P. F. Nealey. *J. Colloid Interface Sci*. **213**, 238 (1999).
65. G. Bogdanovic, A. Meurk, M. Rutland. *Colloids Surf., B* **19**, 397 (2000).
66. A. Feiler, P. Attard, I. Larson. *Rev. Sci. Instrum*. **71**, 2746 (2000).
67. R. G. Cain, M. G. Reitsma, S. Biggs, N. W. Page. *Rev. Sci. Instrum*. **72**, 3304 (2001).
68. A. Feiler, M. A. Plunkett, M. W. Rutland. *Langmuir* **19**, 4173 (2003).
69. M. A. Plunkett, A. Feiler, M. W. Rutland. *Langmuir* **19**, 4180 (2003).
70. S. Zauscher and D. J. Klingenberg. *Colloids Surf., A* **178**, 213 (2001).
71. I. C. Hahn-Berg, M. W. Rutland, T. Arnebrant. *Biofouling* **19** (6), 365–369 (2004).
72. K. Boschkova, A. Feiler, J. Stålgren, B. Kronberg. *Langmuir* **18**, 7930 (2002).
73. Y. Ando. *Wear* **238**, 12 (2000).
74. N. Garoff and S. Zauscher. *Langmuir* **18**, 6921 (2002).
75. A. Homola, J. N. Israelachvili, M. L. Gee, P. M. McGuiggan. *J. Tribol*. **111**, 675 (1989).
76. J. Israelachvili. In *Handbook of Micro/Nanaotribology*, B. Bhushan (Ed.), p. 309, CRC Press, Boca Raton, FL (1995).
77. G. M. McClelland. *Adhesion and Friction*, Vol. 17, Springer, Berlin (1989).
78. M. E. Karaman, L. Meagher, R. M. Pashley. *Langmuir* **9**, 1220 (1993).
79. I. Larson, C. J. Drummond, D. Y. C. Chan, F. Grieser. *J. Am. Chem. Soc*. **115**, 11885 (1993).
80. S. Biggs, M. K. Chow, C. F. Zukoski, F. Grieser. *J. Colloid Interface Sci*. **160**, 511 (1993).
81. S. Biggs and P. Mulvaney. *J. Chem. Phys*. **100**, 8501 1994.
82. S. Biggs, P. Mulvaney, C. F. Zukoski, F. Grieser. *J. Am. Chem. Soc*. **116**, 9150 (1994).
83. M. Prica, S. Biggs, F. Grieser, T. W. Healy. *Colloids Surf., A* **119**, 205 (1996).
84. S. Biggs, P. J. Scales, Y.-K. Leong, T. W. Healy. *J. Chem. Soc., Faraday Trans.* **91**, 2921 (1995).
85. S. Biggs. *Langmuir* **11**, 156 (1995).
86. J. Addai-Mensah, J. Dawe, R. A. Hayes, C. A. Prestidge, J. Ralston. *J. Colloid Interface Sci.* **203**, 115 (1998).
87. A. Feiler, P. Jenkins, J. Ralston. *PCCP* **2**, 5673 (2000).
88. W. Bowen, N. Hilal, R. Lovitt, C. Wright. *Colloids Surf., A* **136**, 231 (1998).
89. W. R. Bowen, A. S. Fenton, R. W. Lovitt, C. Wright. *J. Biotechnol. Bioeng*. **79**, 170 (2002).
90. W. R. Bowen, N. Hilal, R. W. Lovitt, C. J. Wright. *J. Membr. Sci*. **154**, 205 (1999).

91. H. A. Bustamante, S. Raj Shanker, R. M. Pashley, M. E. Karaman. *Water Res.* **35**, 3179 (2001).
92. D. T. Atkins and R. M. Pashley. *Langmuir* **9**, 2232 (1993).
93. I. Larson, C. J. Drummond, D. Y. C. Chan, F. Grieser. *J. Phys. Chem.* **99**, 2114 (1995).
94. L. Meagher and R. M. Pashley. *Langmuir* **11**, 4019 (1995).
95. G. Toikka, R. A. Hayes, J. Ralston. *J. Colloid Interface Sci*. **191**, 102 (1997).
96. S. Veeramasuneni, M. R. Yalamanchili, J. D. Miller. *J. Colloid Interface Sci*. **184**, 594 (1996).
97. I. Larson, C. J. Drummond, D. Y. C. Chan, F. Grieser. *Langmuir* **13**, 2109 (1997).
98. K. Hu and A. J. Bard. *Langmuir* **13**, 5418 (1997).
99. P. Mulvaney, J. M. Perera, S. Biggs, F. Grieser, G. W. Stevens. *J. Colloid Interface Sci.* **183**, 614 (1996).
100. F. Grieser, P. Hartley, P. Mulvaney, G. W. Stevens. *Langmuir* **15**, 7282 (1999).
101. P. D. Ashby, L. Chen, C. M. Lieber. *J. Am. Chem. Soc*. **122**, 9467 (2000).
102. I. Larson, D. Y. C. Chan, C. J. Drummond, F. Grieser. *Langmuir* **13**, 2429 (1997).
103. R. Raitieri, M. Grattarola, H.-J. Butt. *J. Phys. Chem*. **100**, 16700 (1996).
104. A. C. Hillier, S. Kim, A. J. Bard. *J. Phys. Chem*. **100**, 18808 (1996).
105. K. Hu, F.-R. Fan, A. J. Bard, A. C. Hillier. *J. Phys. Chem.* **101**, 8298 (1997).
106. I. Larson and R. J. Pugh. *Langmuir* **14**, 5676 (1998).